Petroleum and Coal

Article **Open Access**

FLUID TRANSPORT PROPERTIES AND CHARACTERIZATION OF WETTABILITY TRENDS OF AGBADA SANDSTONE PETROLEUM RESERVOIR

Onuoha F. Wopara[1,2] and Sunny E. Iyuke[2]

[1] Department of Petroleum Engineering, Rivers State University, Port Harcourt, Nigeria
[2] School of Chemical and Metallurgical Engineering, University of the Witwatersrand, Johannesburg, South Africa

Received June 7, 2017; Accepted September 22, 2017

Abstract

Knowledge of the properties that govern the flow of fluids through a petroleum reservoir is very critical to understanding flow dynamics at the pore-scale and designing of efficient oil recovery plans. In this work, we used 3-D X-ray images of the rock microstructure of the Agbada sandstone reservoir in the Niger Delta of Nigeria used to determine the porosity, absolute permeability, and relative permeability by simulating fluid flow on 24 core samples using ImageJ software and the Lattice Boltzmann method, respectively. Obtained results were compared with laboratory measured values on the same core plug samples; good agreement was observed between the two sets of values. Wettability of the core samples was measured by the Amott imbibition method and characterized by Amott-Harvey indices. The results showed that samples exhibited water-wet characteristics, confirmed by analysis of the relative permeability curves.

Keywords: Agbada sandstone; digital rock physics; X-ray micro-tomography; pore-network modelling; Lattice Boltzmann simulation.

1. Introduction

Reservoir simulations needed to evaluate different improved oil recovery options require input parameters such as porosity, relative permeabilities, capillary pressures, wettability, and other rock and fluid properties. These parameters are normally derived from core analysis (SCAL) tests that deal primarily with the laboratory determination of petrophysical properties of petroleum reservoir rocks. Core analysis experiments are time-consuming and often are not carried out at reservoir conditions with live reservoir fluids. However, this has been simplified by the application of computer in the analysis, which requires a minimum number of experimental data. Successes in rock pore-space scanning and the use of very powerful, high-performing computer systems have advanced the application of digital rock physics as a tool for the analysis of rock petrophysical properties, simulation of flow of fluids in a given porous medium, and as a back-up to laboratory experimental measurements [1]. Using high-performance computers, a large number of reservoir core samples can be tested at a very short time, and petrophysical properties that otherwise will be difficult to determine with laboratory core analysis can now be estimated with a high degree of certainty [2-3].

Geologists and petroleum engineers rely on recent advances in micro-imaging of natural rocks, combined with advances in pore-scale modelling and simulation to gain better insights into pore-level displacement mechanisms of fluids, relative permeabilities, capillary pressures, reservoir rock wettability, and waterflood oil recovery trend during petroleum exploration, production, and throughout the lifespan of the reservoir [4]. An understanding of the pore structure of petroleum reservoir rock is important in obtaining features which statistically describe the porous medium and is helpful in analyzing the effects of reservoir fluid properties on enhanced oil recovery efficiency.

Recently, high-speed digital computers have found wide application in two-dimensional image processing and classification techniques that are useful for predicting the properties of porous media. High-resolution micro-CT scans can be used for a range of applications in areas such as determination of porosity, specific permeability and formation factor, which are very vital for designing oil recovery processes. Permeability, for example, is a critical parameter in defining the flow capacity of a rock sample. It is a measure of the ability of a porous media to transmit fluids and is therefore critical for modelling fluid flow in porous media. Scan images of rocks and data obtained can show features such as grain size and shape, pore size and pore network, and potentially visualize fluids and their saturations within the rock system. Computer graphic presentations and statistical analyses can reveal significant trends in reservoir quality which are not readily extracted from numerical core data, especially in multi-well studies. Thus, a computer network modelling, where displacement is simulated through a lattice of pores connected by throats, would make predictions of the microscopic fluid distribution as they relate to macroscopic parameters a useful approach to obtain wettability index, rock micro-structure, multiphase flow and oil recovery data [5].

The application of network modelling to explore the effects of wettability on relative permeability and waterflood oil recovery was reported by Kovscek and co-workers [6]. Their work was a confirmation of other works already reported elsewhere [4,7-8]. A digital technique has been applied for directly imaging the pore-scale distribution of fluids in reservoir cores using high-resolution tomography and a newly developed 3D registration technique which allows perfect voxel alignment of a set of images of the same core [9]. Raeini and co-workers, using different rock systems at well-defined wettability states, air and water, demonstrated the applicability of the techniques to study the effect of pore-scale forces on the macroscopic behavior of multiphase flow in porous media. They used a new volume-of-fluid based finite volume method developed for simulating two-phase flow directly on micro-CT images of porous media [10]. Overall, their work presents a new finite volume-based methodology for the detailed analysis of two-phase flow directly on micro-CT images of porous media and upscaling of the results to the Darcy scale. Idowu and co-workers proposed an integrated methodology for determining the pore-scale distribution of wettability of rock samples to guide pore network modelling [11]. Wettability was characterized by spatial registration of rock images from X-ray micro-computed tomography (MCT), Field Emission Scanning Electron Microscopy (FESEM), and Quantitative Evaluation of Minerals by SEM (QEMSCAN). Using mini-plugs of an outcrop and a reservoir sandstone drained and aged in oil, they carried out spontaneous and forced imbibition of brine and acquired x-ray tomogram after each preparation step. Obtained wettability information was then used to assign plausible wettability parameters to pores and throats of topologically equivalent networks. The simulated oil/water displacement results for the reservoir sandstone showed good agreement with available SCAL data.

Detailed x-ray computed tomography studies of the geometry of petroleum reservoir rock pore space, and fluid flow properties have been carried out for relatively homogeneous networks (Fontainebleau, Berea, and Bentheim), which represent a few sandstone reservoir rock systems [12-14]. However, the advent of digital rock physics has made it possible to determine the pore structure of a wide range of rock samples using micro-CT imaging. Digital rock physics provides faster and better analysis of porous reservoir rocks [15].

Despite the hydrocarbon resources potential of the Agbada petroleum reservoir rock, there is the absence of studies in literature dedicated to the determination of the petrophysical properties that govern the flow and transport of fluids through the porous system. In this work, the porosity, permeability, relative permeability and wettability of Agbada sandstone petroleum reservoir rock are determined using digital rock physics (DRP) analysis and laboratory core analysis methods.

2. Agbada petroleum system

The Agbada sandstone petroleum system is situated in the Gulf of Guinea in a rift triple junction related to the opening of the southern Atlantic. It started in the Late Jurassic to the Cretaceous

rock in the Niger delta, ranked among the major prolific deltaic hydrocarbon provinces in the world. It lies on the west coast of Central Africa (South of Nigeria) [16]. Petroleum in the Niger delta is principally produced from sandstones and unconsolidated sands predominantly in the Agbada formation.

The delta is located in West Africa between latitude 30 and 60 N and longitude 50 and 80E (Figure 1). It is of the Eocene age with accumulated sediments well over 10 kilometers thick. It is one of the world's most prolific petroleum producing tertiary deltas that accounts for about 5% of the world's oil and gas reserves and about 2.5% of the present-day basin areas on Earth [18-19]. To date, over 37 billion barrels of recoverable oil and 188 trillion standard cubic feet (SCF) of recoverable gas have been discovered. Mineralogy of the Agbada sandstone indicates the following: quartz ranges from 58 to 85%, albite from 16 to 24%, calcite from 2 to 6%, dolomite from 0.5 to 4%, kaolinite from 2 to 6% and muscovite from 0.5 to 3% [20].

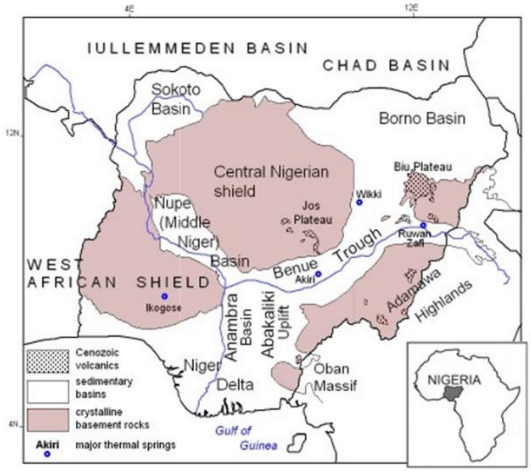

Figure 1. Niger delta geological setting and location of major structural units [17]

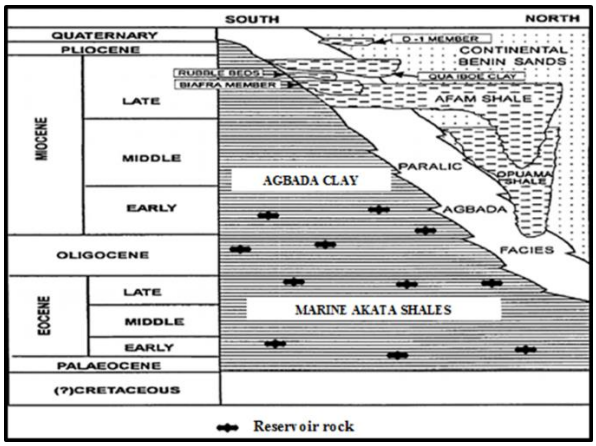

Figure 2. Lithostratigraphical cross section across the Niger Delta [18]

The geology of the tertiary Niger delta is linked to three formations that represent pro-grading depositional facies, identified primarily by sand-shale ratios. The delta's sediments show an upward transition from marine pro-delta thick shales (Akata Formation) believed to be a potential source rock, through a paralic interval (Agbada Formation), the major petroleum-bearing unit, which began in the Eocene and continues into the Paleocene to a continental Late Eocene to Recent sequence of alluvial and upper coastal plain sands (Benin Formation) that are up to 2 kilometres thick [21], Figure 2. These three sedimentary environments, typical of most deltaic environments, extend across the whole delta and ranges in age from early tertiary to resent. Structural traps are the most common traps in Niger delta system. However, stratigraphic traps are not uncommon. The structural traps developed during synsedimentary deformation of the Agbada paralic sequence. A variety of structural trapping elements exists, including those associated with simple rollover structures; clay filled channels, structures with multiple growth faults, structures with antithetic faults, and collapsed crest structures [19].

2.1. Properties of Oil in the Niger delta

The physical and chemical properties of the oil in the Niger delta are highly variable. The oil has a gravity range of 16-50° API, with the lighter oils having a greenish-brown colour [22]. About 56% of Niger delta oils have API gravity between 30° and 40° [23]. The oils are divided into two groups. The first group is light paraffin based, waxy oils from deeper reservoirs, with wax content between 5% and 20%, but commonly around 5%, and high n-paraffin/naphthene of 0.86 [24]. The second group of oils are biodegraded and are found in shallow reservoirs, with lower API gravity, averaging 26° [25]. They are naphthenic non-waxy oils, with n–paraffin/ naphthene of 0.37. Biodegradation and washing in some Pleistocene sands of the Agbada formation result to formation of extra heavy oils, with API of 8-20°. Oils with less than 25° API

account for only 15% of the Niger delta reserves [23]. The concentration of sulphur in most oils is low, between 0.1 % and 0.3 % [26], with a few samples having concentrations as high as 0.6 % [27].

In this paper, we study the petrophysical properties that govern the flow of fluids in the Agbada sandstone hydrocarbon system and its wetting tendency using conventional laboratory methods and digital rock physics analysis. This is significant because not much is available in the literature on the features that define its potentials as a world major hydrocarbon pool. This study will, therefore, provide and/or compliment whatever little data that exist in the public domain on this petroleum system

3. Pore-scale simulation of transport properties

Many hydrocarbon reservoir rocks have different orientations and matrix block sizes [28]. This creates complexity in multiphase porous media flow and makes modelling and calculation of transport properties very difficult. Laboratory experiments are slow and costly, and empirical relations have not proved to be always effective for complex multiphase flow processes. With the increase in modern computing power, numerical simulation techniques have gained increased application as an alternative to solving porous media flow. The lattice Boltzmann method (LBM) is an attractive and powerful numerical tool that has found wide application for pore-scale simulation of multiphase flows in porous media [29-34]. LBM is used to simulate complex multiphase flows in domains with realistic pore geometries. In the LBM, simplified kinetic models are derived that incorporate the essential physics of fluid flow processes in the pore spaces of the rock microstructure to ensure that the macroscopic averaged properties are in conformity with the desired constitutive mathematical relationships. The LBM is simple in implementation and robust and has the capability to handle single-phase, two-phase and multi-component flows in complex three-dimensional geometries, such as porous media without over-simplification of the pore [35-41]. It can solve the Navier-Stokes equation accurately with real pore geometries. It has been shown that the LBM can give an accurate solution equivalent to the one by the finite-element and finite-difference methods [38,42-43] without extensive meshing. Moreover, most operations in the LBM are local. Thus, it reproduces interface between multiple phases with flexibility and is ideal for parallel implementation. Liu *et al.* [34] give a detailed review of some multiphase simulation models based on LBM that have been used to model flows at the pore-scale level. In this work, the lattice Boltzmann method (LBM) is used to simulate pore-scale flow for the permeabilities of the Agbada sandstone core samples.

4. Experimental methods

4.1. Core samples

Experiments were performed on twenty-four (24) whole reservoir core samples taken from different oil bearing Agbada sandstone formations. The fields from which these samples were taken are identified as A to L. Two samples were taken from each field, representing various well depths and lithology. For example, cores A1 and A2 are taken from two oil wells at different depths in a field.

Fig. 3. Agbada sanstone reservoir core plugs used in this work

Twenty four (24) core plugs of approximately 3 inches in length and 1.5 inches in diameter each were cut from these whole cores. Figure 3 shows samples of the sandstone core plugs used in the experiments in this work. After trimming, the plugs' edges were cleaned of fines using the Acetate Peel method.

4.2. Image scanning, segmentation, and network extraction

In this work, 3D micro-CT images of the Agbada sandstone core samples were generated using a 'v|tome|x' high-resolution desktop scanner located in the XMT laboratory at the Department of Materials, Imperial College London. v|tome|x, manufactured by Phoenix|x-ray in Germany is equipped with an image acquisition and processing software, SIXTOS, and a 100 kV X-ray source. The X-ray images were generated at 90kV tube voltage, a current of 100 μA and a 0.5 mm Al filter. The rotation increment was 0.5 for a full 360^0 rotation. The 16-bit digital X-ray detector of this system is a flat panel detector, Perkin Elmer RID 512-400, based on an 8" amorphous silicon sensor with a pixel size of 400μm and a field of view of 512 × 512 pixels. The micro-CT scans, therefore, provide gray-scale images, which relate to the density of the analysed material.

The 3-D μCT grayscale images were segmented using thresholding along the image boundaries (edge thresholding) technique instead of the histogram thresholding method. It has been shown that histogram thresholding method results to porosity value higher than the real porosity of rock core samples [44-45]. Using this technique was therefore not considered accurate for calculation of porosity of the rock samples examined in this work. Thresholding along boundaries results in porosity values, closer to the real porosity of the rock. Therefore, this technique was recognized as the best for rock's porosity evaluation. Segmentation is carried out to expose the rock mineral contents, clays and, principally, to distinguish grain (1) from pore space (0) or void [46-49]. The micro-CT images obtained were post-processed to give 3-D digital models of the scanned rock samples for use in numerical fluid flow simulations to obtain permeabilities. Maximal ball algorithm was used to extract topologically equivalent network of the rock [50-51]. The extracted pore network was used to compute porosity, absolute and relative permeability and the results obtained were compared to laboratory measured values. The same core plugs used for image scan analysis were also used for laboratory measurements of porosity, absolute and relative permeability measurements. Properties of the fluids used in the experiments are shown in Tables 1 and 2.

Table 1. Water composition

Iron	Na^+	Ca^{2+}	Mg^{2+}	K^+	Cu^{2+}	Ba^{2+}	SO_4^{2-}	Cl^-
Conc. (g/L)	77.8	24.1	3.1	2.8	0.002	0.179	0.13	151

Table 2. Properties of crude oils

Oil Sample	Density (g/cm^3)	Viscosity @ 50°C, (cP)	Acid number (mgKOH/g Oil)	Base Number (mgKOH/g Oil)
Bonny Light	0.8479	2.8	0.221	0.08
Forcados Blend	0.8811	3.4	0.237	0.17

4.3. Numerical calculations

4.3.1. Porosity

The x-ray images of the samples were exported to a computer, and MATLAB 7.0 Image Processing software was used to quantify the results. MATLAB Image Processing Toolbox™ provides a comprehensive set of reference-standard algorithms, functions, and apps for image processing, analysis, visualization, and algorithm development. We can perform image analysis, image segmentation, image enhancement, noise reduction, geometric transformations, and image registration. Many toolbox functions support multicore processors, GPUs, and C-code generation. Image Processing Toolbox supports a diverse set of image types, including high dynamic range, gigapixel resolution, embedded ICC profile, and tomographic. Visualization functions and apps allow the exploration of images and videos, examine a region of pixels, adjust colour and contrast, create contours or histograms, and manipulate regions of interest (ROIs). The toolbox supports workflows for processing, displaying, and navigating large images.

Using the segmented version of the micro-CT-scan, total porosity is estimated by the equation:

$$\varphi_t = \frac{V_p}{V_r} \quad (1)$$

where V_p is the pore space area in the segmented image and V_r the total area of the rock matrix. In terms of dimensionality and pixel resolution, equation (1) is rewritten in terms of pixel count as:

$$\varphi_t = \frac{N_{pp}}{N_{tp}} x100\% \quad (2)$$

where N_{pp} is the pore space pixel count and N_{tp} the total number of pixels.

As stated earlier, for comparison, the porosity of the rock core samples was measured in the laboratory using the helium porosimeter. This method relies on the expansion of helium gas, employing Boyle's law in a closed system under isothermal conditions. Helium is most often preferred as the measurement gas because it is an inert gas, with creeping little molecules that can penetrate even the smallest voids or pores without adsorbing on the rock surface. Table 3 shows the values of porosity measured in the laboratory and those calculated from the pore network and the corresponding calculated percentage errors or deviations for the dataset.

Table 3. Experimental and calculated porosity values

Core ID / Porosity	A1	A2	B1	B2	C1	C2	D1	D2	E1	E2	F1	F2
Network values	28.9	27.8	28.6	27.8	28.2	27.0	27.3	26.5	28.1	27.3	29.5	27.9
Experimental values	29.4	28.3	29.2	28.3	28.8	28.5	27.6	26.9	28.6	27.7	30.0	28.1
% Error	1.7	1.8	2.1	1.8	2.1	1.8	1.1	1.5	1.8	1.5	1.7	0.7
Core ID / Porosity	G1	G2	H1	H2	I1	I2	J1	J2	K1	K2	L1	L2
Network values	30.1	27.7	29.2	27.0	28.7	27.5	29.8	27.4	28.6	27.0	28.5	27.3
Experimental values	30.6	28.2	28.6	27.5	29.1	28.0	31.3	27.8	28.3	27.4	29.0	27.8
% Error	1.7	1.8	(2.0)	1.9	1.4	1.8	1.7	1.5	(1.0)	1.5	1.8	1.8

4.3.2. Absolute permeability

Many workers have used Lattice-Boltzmann as a pore-scale numerical method, in conjunction with network modelling, to accurately estimate absolute and relative permeability [52-55]. In this work, the lattice Boltzmann method (LBM) was used to simulate fluid flow for the absolute permeability of the core samples. Known for its ability to handle complex geometries (boundary conditions) LBM, compared to traditional computational fluid dynamics (CFD), models the fluid as consisting of fictitious particles performing consecutive propagation and collision processes on the discrete lattice mesh (voxel grids), rather than solving numerically for the conservation equations of mass and momentum without solving the Navier-Stokes equation directly at the continuum level [56-58]. Absolute permeability is then calculated using the same concept used in Darcy's experiment and expressed by Darcy's law, written as:

$$Q = \frac{kA}{\mu}\frac{(P_1 - P_2)}{L} \quad (3)$$

where Q is the flow rate of the fluid through the porous medium (cm^3/s); P_1 is the fluid pressure at the inlet (Pa); P_2 is the fluid pressure at the outlet (Pa); μ is the dynamic viscosity of the fluid (Pa.s); L is the length of the porous medium (m); k is the permeability of the sample (Darcy or m^2); and A is the cross-sectional area of the sample (m^2).

Zhang *et al.* [59] used the Lattice Boltzmann (LB) method to solve for single-phase flow in complex geometries. Degruyter *et al.* [60] developed a tool based on LBM to calculate permeability, with the application of the solver Palabos. The Palabos library is a framework for general-purpose computational fluid dynamics (CFD), with a kernel based on the Lattice Boltzmann (LB) method. Its programming interface (C++) is straightforward and makes it possible to set

up fluid flow simulations with relative ease. From the simulation, permeability can be calculated by relating the total flux to the pressure gradient over the length of the sample using the following equation to conform to Palabos [61]:

$$k = \frac{\langle v \rangle \mu}{dP/_{dL}} \quad (4)$$

where $\langle v \rangle$ is the average magnitude of the intrinsic velocity over the entire network or system.

The 3-D 19 velocity (D3Q19) model [62] and the Parallel Lattice Boltzmann Solver, Palabos (http://www.lbmethod.org/palabos), with multiple relaxation time (MRT), periodic boundary conditions and free fluid layer were applied to conduct the fluid flow simulation [63-64]. To calculate permeability in each direction (x, y, z), a no-flow (no-slip) boundary condition was imposed at the rock/fluid interface parallel to the main flow direction, and zero pressure gradients across the sample, i.e., fixed pressures at the inlet and outlet of the core sample, respectively. Experimental measured absolute permeability and network simulated values are shown in Table 4.

Table 4. Experimental and network simulated absolute permeability values

Core ID / Absolute k(md)	A1	A2	B1	B2	C1	C2	D1	D2	E1	E2	F1	F2
Network simulation average values	1791	1786	1780	1774	1654	1650	1589	1585	1761	1782	1782	1778
Experimental values	1802	1794	1786	1780	1693	1655	1627	1669	1770	1766	1780	1782
Core ID / Absolute k(md)	G1	G2	H1	H2	I1	I2	J1	J2	K1	K2	L1	L2
Network simulation average values	1808	1773	1880	1765	1790	1703	1672	1610	1784	1708	1725	1681
Experimental values	1813	1778	1884	1770	1802	1709	1676	1614	1789	1712	1710	1686

4.3.3. Porosity/permeability cross-plots

Next, the laboratory measured and network calculated porosity and permeability values are cross-plotted on a linear scale. The cross-plots are shown in Figures 5, 6 and 7.

4.3.4. Relative permeability

Relative permeability through reservoir rocks is affected by the pore space geometry, flow conditions, saturation history, and wettability. However, the relative permeability is assumed to be saturation-dependent only. The simulations are carried out using a 200^3 sub-volume extracted from the CT scan of the Agbada rock. In this paper, a mixture velocity (with fixed oil/water ratio) was imposed at the core inlet. The pressure at the outlet was also fixed, resulting in zero capillary pressure at the outlet. This boundary condition is widely used in special core analysis simulations.

The fluid properties are indicated in Table 2, the interfacial tension between oil and water phases, $\sigma_{w,0}$, is 25 dynes/cm. An equilibrium contact angle of θ = 30^0 and a fixed capillary number, Ca, of 2.5 x 10^{-5}, typical values used in experimental steady-state measurements, were assigned in this work. The core sample was initially filled with water. Once equilibrium was reached for every oil/water injection ratio regarding oil saturation S_o and pressure, the simulated relative permeability data for oil, k_{rw} and water, k_{ro}, were calculated using the Brooks-Corey-Burdine empirical relationship [65-66]:

$$k_{rw} = S_{ew}^4,$$
$$k_{ro} = (1 - S_{ew})^2(1 - S_{ew}^2), \quad (5)$$
$$S_{ew} = \frac{S_w - S_{rw}}{1 - S_{rw}}$$

where k_{rw} and k_{ro} are the water and oil relative permeability, respectively; S_{ew}, S_{rw}, and S_w are the effective saturation of the water phase, residual saturation of the water phase, and the saturation of the water phase, respectively.

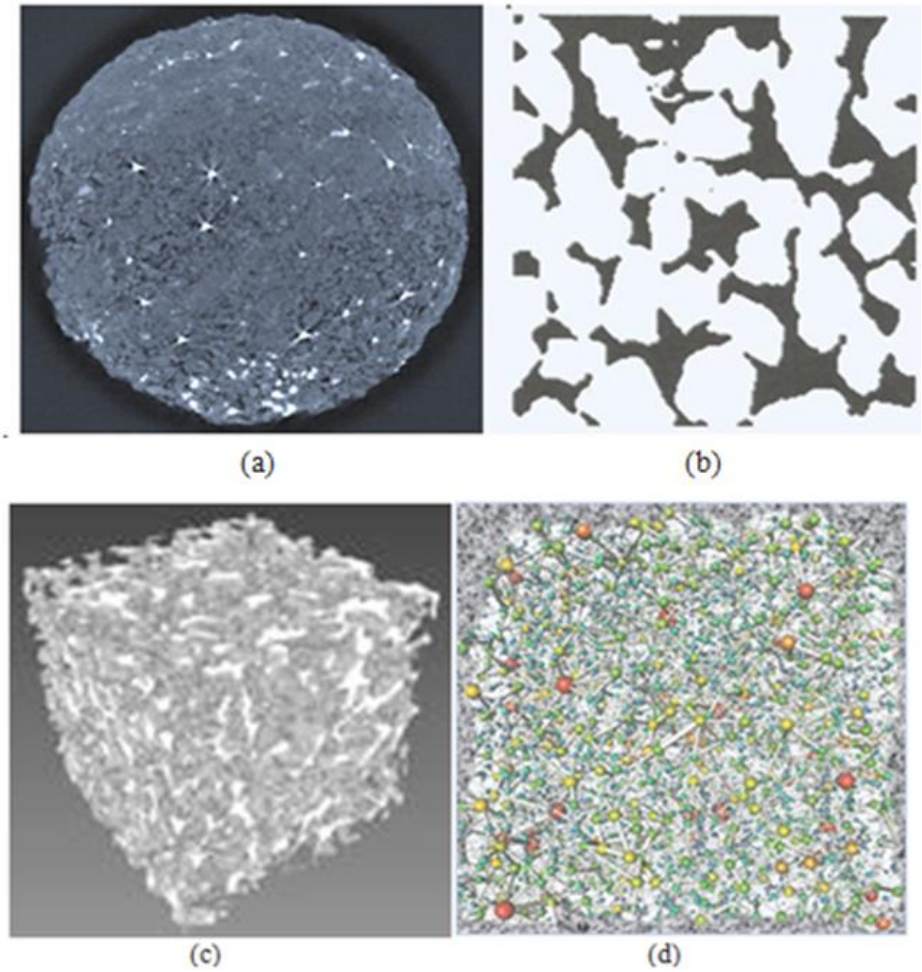

Figure 4. (a) 2-D cross-section of an Agbada core sample (sample B). Image size (in voxels) is 512 x 512 x 400 mm, resolution is 8 microns. Actual image size is 4.1 x 4.1 x 3.2 mm^3; (b) segmented image with the pore space in black and the solid in white. (c) 3-D image of the pore space after segmentation on a small volume of 200^3 voxels (d) the extracted network [50]

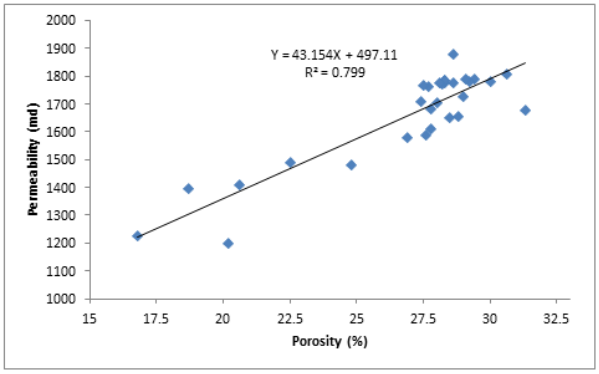

Figure 5. Experimental measured permeability/ porosity linear relationship of 24 core samples of Agbada sandstone formation

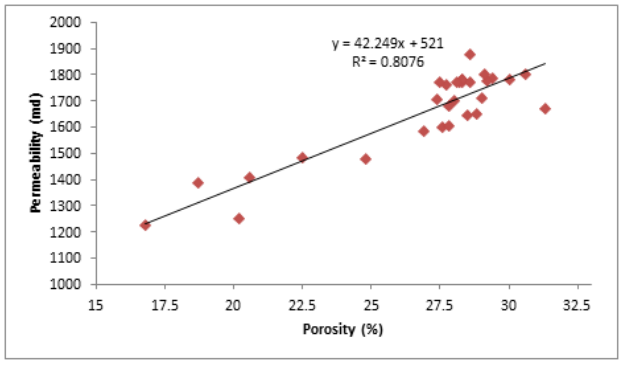

Figure 6. Simulated permeability/porosity linear relationship of 24 core samples of Agbada sandstone formation

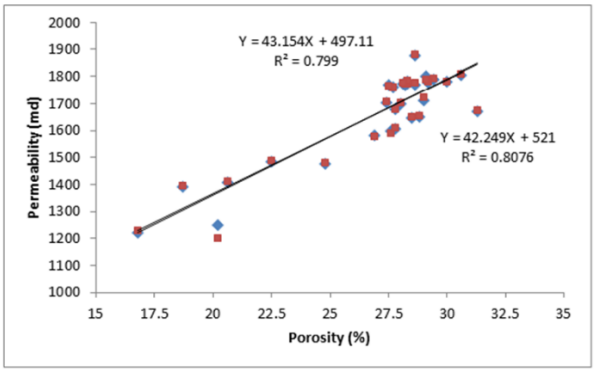

Figure 7. Combined experimental and simulated permeability/porosity linear relationship for 24 core samples of Agbada sandstone formation

The simulation was carried out at very low fluid velocities to achieve low Reynolds numbers (Re) typical of Darcy (laminar) flow. The simulated data were compared with the experimental data obtained from the same core samples using laboratory waterflood method [45]. Figure 8 shows the relative permeability curves for the two sets of data for oil (red and purple) and water (blue and green). The purple and green colour curves represent relative permeabilities calculated from the numerical simulation, while the red and blue colour curves represent the experimental data.

4.3.5. Wettability measurement

A lot of work exists in the literature on the importance and effect of wettability of reservoir rocks on the spatial distribution of fluids in a porous medium and on fluid transport properties, such as relative permeability, capillary pressure, enhanced oil recovery during water/gas injection, irreducible water saturation and residual oil saturation [67-71]. This paper will not discuss these works but rather will characterise the wettability trend of the Agbada sandstone petroleum rock using the Amott-Harvey method and relative permeability curve analysis. In the Amott method, three deferent wettability indices were measured: 1) Water wettability index, I_w, which is the ratio of V_{osi} to (V_{osi} + V_{ofi}); 2) Oil wettability index, I_o, which is the ratio of V_{wsi} to (V_{wsi} + V_{wfi}); and 3) Amott-Harvey wettability index, $I_{w\text{-}o}$, which is the difference between I_w and I_o.

Five (5) reservoir rock core plug samples from different Agbada oil producing fields were used for spontaneous and forced imbibition process to determine wettability of the system. The samples were cleaned by Distillation/Extraction method [72] using a Dean Stark and Soxhlet Extractor. Toluene was used as the cleaning solvent. The cleaned samples were dried in an oven at a temperature of 110^{0}C for 60 hours.

Table 5. Measured properties of the core samples

Core ID	AO2	BI1	CG2	DY1	EM1
Length, cm	7.78	7.80	7.76	7.81	7.82
Diameter, cm	3.83	3.81	3.83	3.82	3.82
Porosity. %	27.2	28.1	28.3	27.8	28.2
Permeability, md	1780	1688	1720	1675	1736

Results of the porosity and absolute permeability of the samples measured in the laboratory are shown in Table 5. After preparation, the samples were restored to reservoir wettability state for spontaneous imbibition experiments. The clean and dry core plugs were first saturated with reservoir oil (Bonny Light Oil) in a vacuum pump setup for 1 hour. In order to restore reservoir wettability, the samples were then aged for 40 days by submerging in the reservoir oil at 90^{0}C.

The fully saturated core plugs were placed in Amott imbibition cells under ambient conditions, surrounded by brine for 7 days to attain equilibrium. Brine imbibed into the matrix of the core plugs displacing oil, which ascends to a graded cylinder at the top of the cell. After equilibrium was reached the total volume of oil displaced with time was recorded for each system. The cores were then taken out of the cells, quickly dried, weighed and centrifuged for about 1 hour to force the remaining oil down to residual saturation. After that, the cores were saturated with brine at residual oil saturation, placed in Amott drainage cells and surrounded by oil for 7 days to allow for spontaneous drainage. The procedure is summarized in the following 5 steps:

1) Establish S_{wir}

2) Submerge the specimens in water and record the volume of oil produced
3) Centrifuge the specimens in water and record the volume of oil produced
4) Submerge the specimens in oil and record the volume of water produced
5) Centrifuge the specimens in oil and record the volume of water produced

Results of Amott-Harvey index measurements for five of the core plug samples are shown in Table 6 while a plot of spontaneous imbibition rates is shown in Figure 9

Table 6. Results of the Amott-Harvey displacement index for the 5 core samples

Core ID	AO2	BI1	CG2	DY1	EM1
Spontaneous oil production, (Step 2)	8.20	7.68	9.00	8.02	7.12
Forced oil production, (Step 3)	1.78	1.92	0.90	1.04	0.12
Spontaneous oil production, (Step 4)	0.2	0.12	0.09	0.04	0.14
Forced water production, (Step 5)	8.7	6.64	7.84	6.10	6.86
Water Wettability index $I_w=2/(2+3)$	0.82	0.80	0.91	0.89	0.98
Oil Wettability index $I_o=4/(4+5)$	0.02	0.02	0.01	0.01	0.02
Amott+Harwey Index $I_{w-o}=I_w-I_o$	0.80	0.78	0.90	0.88	0.96

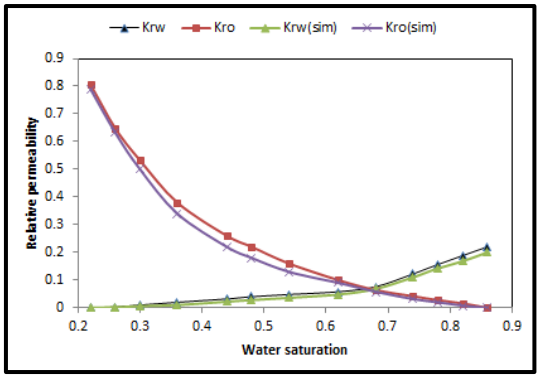

Figure 8. Comparison of simulated and experimental relative permeabilities

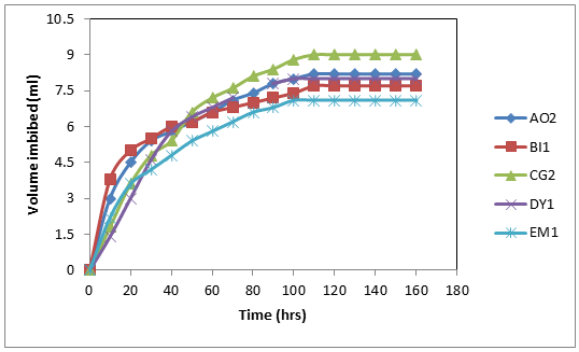

Figure 9. Plot of spontaneous imbibition rates for the core samples

4.3.6. Relative permeability and saturation curves

In order to further validate the water-wet characteristics of the Agbada sandstone petroleum reservoir, plots of the results of the relative permeability measurements for the core samples before and after wettability alteration by aging were plotted. The plots are shown in Figures 10 and 11.

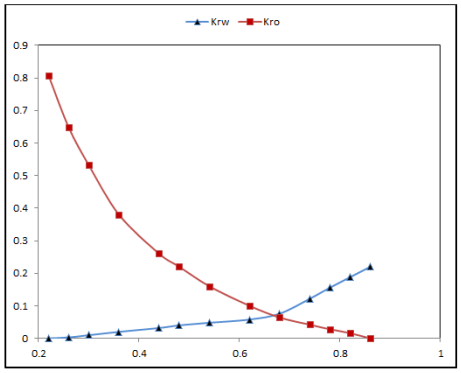

Figure 10. Plot of experimental relative permeability values before wettability alteration

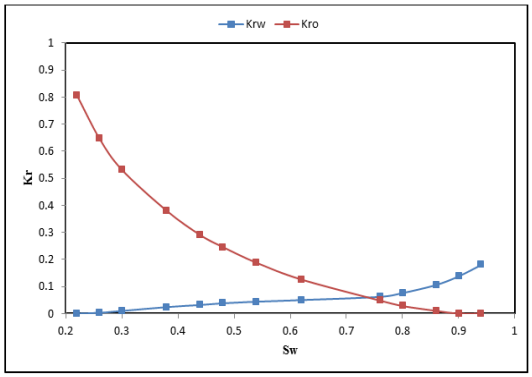

Figure 11. Plot of relative permeability after wettability alteration

5. Discussion of results

Image scanning and experimental calculation methods have been applied to evaluate the porosity, absolute and relative permeabilities of the Agbada sandstone reservoir rock. Fluid flow was modeled on micro-CT images of core samples taken from the Agbada sandstone reservoir. The image scanning procedure is based on direct analysis of micro-CT 3-D images of the rock pore space. All the images have 512 x 512 x 400 mm voxels. The 3-D μ-CT images and the resulting pore network, generated using the maximal ball algorithm, are shown in Figure 3. Permeability was calculated from Darcy's law using the flow rate, Q, the applied pressure gradient, ΔP, viscosity of the fluid, μ, the length of the system in the main direction of flow over which pressure gradient was applied, L_x, and the area of the face normal to the main direction of flow, A_x. Resolution of micro-CT images used for flow simulation is 8 μm.

Porosity values obtained by laboratory experiments and network calculations respectively are shown in Table 3. Comparing the two sets of data, it can be seen that the pore network-calculated porosities are a little smaller than the porosities measured by laboratory core analysis. This is because only the porosity of connected pores and throats was counted by CT technique and liquids could not flow into some very small pores and throats. However, porosity calculated from analytical (laboratory experiment) and DRP simulations are generally in close agreement. This close match confirms the reliability of the data obtained by X-ray CT method. The same can be said for the absolute permeability values obtained by laboratory measurements which show reasonable agreement with the averaged pore network simulation values (Table 4).

On Figures 5 and 6 it is observed that some of the data points on the porosity/permeability cross-plots deviate from the actual porosity and permeability of the samples. Despite the deviations, there is a distinctive trend that indicates a close match between the computed and the laboratory measured values (Figure 7). An important practical implication of this is that it is possible to obtain a valid permeability/porosity trend from small, statistically under-representative micro-CT images of rock fragments that are unsuitable for standard laboratory measurements, particularly in unconsolidated and medium-consolidated sandstone formations by using a significant number of such small fragments. Then it may be possible to establish a suit of a site-specific permeability-porosity trend for estimating absolute permeability from independent porosity data, obtained from analysis of well logs or seismic data.

The plots of simulated relative permeabilities and experimental relative permeabilities are shown in Figure 8. Analysis of the plotted relative permeability data for both cases shows that the pore network simulation results are in very close agreement with the experimental curves both for the cross-over points and the end-points.

Spontaneous imbibition experiments were conducted on 5 core samples using the Amott-Harvey method in order to characterize the wetting trend of the sandstone reservoir. The imbibition experiments show that the initial wettability of the reservoir core samples after restoration by aging exhibited water-wet characteristics. This is verified by the rock imbibing the pure reservoir brine spontaneously, indicated by the positive values of the Amott-Harvey indices (Table 6). The relative permeabilities of the wetting phase for brine system are lower than the relative permeabilities of the wetting phase for the oil system, while it is the opposite for the non-wetting phase relative permeabilities. This shows that altering the wettability of the core samples from water-wet to oil-wet increases the relative permeability of the wetting phase, indicating the effect of wettability alteration on oil recovery from the reservoir. As the water saturation increases, the water-to-oil relative permeability ratio increases. Also, the trend in relative permeability relationship to phase saturations observed in Figures 10 and 11 shows that for all values of water saturation above the initial water saturation, the relative permeability to water decreases with increasing water-wetness. Beyond the cross-over values, the relative permeability to water at the same saturation increases while that to oil decreases towards zero. The cross-over saturations of the samples for water and oil are more than 0.5. This is considered as an indication of water wetness of the Agbada sandstone formation.

6. Conclusions

This paper has carried out the study on the determination of the fluid flow properties of porosity, permeability, relative permeability and wetting characteristics of Agbada sandstone petroleum reservoir rock using digital rock physics analysis. Results show that the values of these properties obtained by pore network simulation are validated by laboratory experimental measured values. The mechanism of spontaneous imbibition of water by sandstone cores was also studied. Results indicate that the Agbada sandstone petroleum rock exhibited water-wet characteristics.

Small fragments of medium- to high-porosity sandstones that are not statistically representative of a larger sample is not adequate to be used to numerically calculate the true porosity and permeability of the sample. However, using a large number of these small under-representative fragments, it is possible to establish a suit of a site-specific permeability porosity trend for estimating absolute permeability from independent porosity data, obtained from analysis of well or seismic data.

The close match between the pore network-derived and experimental measured relative permeability curves is a confirmation of the capability of pore network/DRP simulations as a tool for accurate prediction of porous media properties. However, it must be stated that the results obtained in this work are not generally an accurate representation of the rock properties of the Agbada reservoir. Rather, they highlight the impact of digital rock physics in the characterization of the properties that govern the flow and transport of fluids in the porous medium. Additional samples of real and reconstructed rock samples need to be systematically investigated to accurately establish qualitative and quantitative trends in the geometric, transport, and petrophysical properties of the rock and trends in storage capacity and flow efficiency of the Agbada petroleum rock system.

Acknowledgements

This work was supported by the National Research Foundation (NRF) of South Africa under the 'Incentive' grant. We express appreciation to the micro-CT system Laboratory of Imperial College London, and in particularly, Dr. Hu Dong who assisted in the scanning of the Agbada rock samples and Professor Martin Blunt for his explanations on pore-scale modeling.

References

[1] Renard P, Genty A, Stauffer F. Laboratory determination of the full permeability tensor. Journal of Geophysical Research 2001; 106: 443.

[2] Andrew M, Bijeljic B, Blunt MJ. Pore-scale imaging of geological carbon dioxide storage under in situ conditions. Geophysical Research Letters 2013; 40: 3915.

[3] Andrä H, Combaret N, Dvorkin J, Glatt E, Han J, Kabel M, Keehm Y, Krzikalla F, Lee M, Madonna C, Marsh M, Mukerji T, Saenger EH, Sain R, Saxena N, Ricker S, Wiegmann A, Zhan X. Digital rock physics benchmarks—part II: Computing effective properties. Computers & Geosciences, 2013; 50: 33.

[4] Blunt MJ. Physically-based network modelling of multiphase flow in intermediate-wet porous media. Journal of Petroleum Science and Engineering, 1998; 20: 117.

[5] Zhao X, Blunt MJ, Yao J. Pore-scale modelling: Effects of wettability on waterflood oil recovery. Journal of Petroleum Science and Engineering, 2010; 71: 169.

[6] Kovscek AR, Wong H, Radike CJ. A pore-level scenario for the development of mixed wettability in oil reservoirs. AIChE Journal, 1993; 39: 1072.

[7] Øren PE, Bakke S, Arntzen OJ. Extending predictive capabilities to network models. SPE Journal, 1998; 3: 324.

[8] Dixit AB, McDougall SR, Sorbie KS, Buckley JS. Pore-scale modelling of wettability effects and their influence on oil recovery. SPE Reservoir Engineering, 1999; 2: 25.

[9] Kumar M, SendenT, Knackstedt MA, Latham SJ, Pinczewski V, Sok RM, Sheppard AP, Michael L. Imaging of pore scale distribution of fluids and wettability. Paper presented at the International Symposium of the Society of Core Analysts 2008, Abu Dhabi, UAE.

[10] Raeini AQ, Blunt MJ, Bijeljic B. Direct simulations of two-phase flow on micro-CT images of porous media and upscaling of pore-scale forces. Advances in Water Resources, 2014; 74: 116.
[11] Idowu N, Long H, Øren P-E, Carnerup AM, Fogden A, Bondino I, Sundal L. Wettability analysis using micro-CT, FESEM and QEMSCAN, and its applications to Digital Rock Physics. Paper presented at the International Symposium of the Society of Core Analysts 2015, St. John's Newfoundland and Labrador, Canada.
[12] Thovert JF, Yousefian F, Spanne P, Jacquin CG, Adler PM. Grain reconstruction of porous media: application to a low-porosity Fontainebleau sandstone. Physical Review E, 2001; 63: 061307.
[13] Blunt MJ, Bijeljic B, Dong H, Gharbi O, Iglauer S, Mostaghim P, Paluszny A, Pentland C. Pore-scale imaging and modelling. Advances in Water Resources, 2013; 51: 197.
[14] Thovert JF Adler PM. Grain reconstruction of porous media: application to a Bentheim sandstone. Physical Review E, 2011; 3: 056116.
[15] Rassenfoss S. Digital rocks out to become a core technology. Journal of Petroleum Technology, 2011; 63: 36.
[16] Aizebeokhai AP, Olayinka I. Structural and stratigraphic mapping of Emi field, offshore Niger Delta. Journal of Geology and Mining Research, 2011; 3: 25.
[17] Kurowska E, Schoeneich K. Geothermal Exploration in Nigeria. Proceedings of World Geothermal Congress 2010, Bali, Indonesia.
[18] Jubril MA, Amajor LC. The Afam clay member; a Lower Miocene incised channel in the South-Eastern Niger Delta. Marine and Petroleum Geology, 1991; 8: 63.
[19] Adedapo JO, Ikpokonte AE, Schoeneich K, Kurowska E. An estimate of oil window in Nigeria's Niger Delta basin from recent studies. American International Journal of Contemporary Research, 2014; 4: 114.
[20] Tuttle LWM, Charpentier RR, Brownfield EM. The Niger Delta Petroleum System: Niger Delta Province, Nigeria Cameroon, and Equatorial Guinea, Africa. U. S. Geological Survey Open File Report 99-50H, Denver, Colorado 1999, 70.
[21] Pusey WC. How to evaluate potential gas and source rocks. World oil 1973, 176: 71.
[22] Whiteman AJ. 1982. Nigeria: Its Petroleum Geology, Resources and Potentials. Vol. 1, Graham and Trotman Publisher, London, UK., 1982, 1, Pages: 394.
[23] Thomas D. 1995. Niger Delta oil production, reserves, field sizes assessed. Oil Gas J,. 1995; 93: 101-104.
[24] Doust H, Omatsola E. Niger Delta, in, Edwards, J. D., and Santogrossi, P.A., eds., Divergent/ passive Margin Basins, AAPG Memoir 48 1990, Tulsa, American Association of Petroleum Geologists, 239-248.
[25] Kulke H. Nigeria. In Regional Petroleum Geology of the World, Part II: Africa, America, Australia and Antarctica, Kulke, H. (Ed.). Gebruder Borntraeger Publ.1995, Berlin, Germany, 143-172.
[26] Mbendi, 1996, http://mbendi.co.za/cyngoi.html (accessed on 15 February, 2017)
[27] Nwachukwu JI, Oluwole AF, Asubiojo OI, Filby RH, Grimm CA, Fitzgerald SA. Geochemical Evaluation of Niger Delta Crude Oils. In Geology of Deltas, Oti, M.N. and G. Postma (Eds.). A.A. Balkema Publ., 1995, Rotterdam, The Netherlands, 287-300.
[28] Bear J. Dynamics of Fluids in Porous Media. New York: American Elsevier 1972.
[29] Pan C, Hilpert M, Miller C. Lattice-Boltzmann simulation of two-phase flow in porous media. Water Resour. Res., 2004; 40: W01501.
[30] Sukop MC, Or D. Lattice Boltzmann method for modeling liquid–vapor interface configurations in porous media. Water Resour. Res., 2004; 40: W01509.
[31] Pazdniakou A, Adler P. Dynamic permeability of porous media by the lattice Boltzmann method. Advances in Water Resources, 2013; 62: 292.
[32] Huang H, Lu XY. Relative permeabilities and coupling effects in steady-state gas-liquid flow in porous media: A lattice Boltzmann study. Phys. Fluids, 2009; 21: 092104.
[33] Liu H, Valocchi AJ, Kang Q, Werth C. Pore-scale simulations of gas displacing liquid in a homogeneous pore network using the lattice Boltzmann method. Transp. Porous Media, 2013; 99: 555.
[34] Liu H, Kang Q, Leonardi CR, Jones BD, Schmieschek S, Narváez A, Williams JR, Valocchi AJ, Harting J. Multiphase lattice Boltzmann simulations for porous media applications-A review. Comput. Geosci., 2016; 20: 777.

[35] Succ, S. The Lattice Boltzmann Equation for Fluid Dynamics and Beyond. Oxford University Press, UK 2001.
[36] Boek ES, Venturoli M. Lattice-Boltzmann studies of fluid flow in porous media with realistic rock geometries. Comput. Math. Appl., 2010; 59: 2305–2314.
[37] Cancelliere A, Chang C, Foti E, Rothman D, Succi,S. The permeability of a random medium: Comparison of simulation with theory. Physics of Fluids A, 1990; 20: 2085.
[38] Ladd A. Numerical simulations of fluid particulate suspensions via a discretised Boltzmann equation (Parts I & II). Journal of Fluid Mechanics, 1994; 271: 285.
[39] Martys NS, Chen H. Simulation of multicomponent fluids in complex three-dimensional geometries by the lattice Boltzmann method. Physical Review E, 1996; 53: 743.
[40] Koponen A, Kandhai D, Hellén E, Alava A, Hoekstra AG, Kataja M, Niskanen K, Sloot P, Timonen K. Permeability of three-dimensional random fiber webs. Physical Review Letters, 1998; 80: 716.
[41] Wu ZS, Dong PC, Lei G, Yang S, Cao N. Lattice Boltzmann simulation of fluid flow in complex porous media based on CT image. Journal of Industrial and Intelligent Information, 2016; 4: 65.
[42] Kandhai D, Vidal DJ-E, Hoekstra AG, Hoefsloot H, Iedema P, Sloot PMA. A comparison between lattice-Boltzmann and finite-element simulations of fluid flow in static mixer reactors. International Journal of Modern Physics, 1998; 9: 1123.
[43] Kandhai D, Vidal DJ-E, Hoekstra AG, Hoefsloot H, Iedema P, Sloot PM. A. Lattice-Boltzmann and finite-element simulations of fluid flow in a SMRX static mixer reactor. International Journal of Numerical Methods in Fluids, 1999; 311: 1019.
[44] Chen A, Wittman T, Tartakovsky A, Bertozz A. Image segmentation through efficient boundary sampling. Appl Math Res Express, 2011; 2: 182.
[45] Wopara OF. Pore network modelling of wettability effects on waterflood oil recovery from Agbada sandstone formation in the Niger delta. PhD Thesis, University of the Witwatersrand, Johannesburg 2016.
[46] Turner ML, Knufing L, Arns CH. Three-dimensional imaging of multiphase flow in porous media. Physica A, 2004; 4: 166.
[47] Arns CH, Bauget F, Limaye A, Sakellariou A, Senden TJ, Sheppard A. P. Pore-scale characterization of carbonates using x-ray micro-tomography. SPE Journal, 2005; 10: 475.
[48] Arns JY, Sheppard AP, Arns CH, Knackstedt MA, Yelkhovsky A, Pinczewski WV. Pore-level validation of representative pore networks obtained from micro-CT images Proceedings of the annual symposium of the Society of Core Analysis, 2007; SCA2007-A26, Calgary, Canada.
[49] Knackstedt M, Jaime P, Butcher AR, Botha PWK, Middleton J, Sok R. Integrating reservoir characterization: 3D dynamic, petrophysical and geological description of reservoir facies. Proceedings of the SPE Asia Pacific oil and gas conference and exhibition, 18–20 October 2010, Brisbane, Queensland, Australia, SPE 133981.
[50] Dong H. Micro-CT imaging and pore network extraction. PhD Thesis, Imperial College, London 2007.
[51] Dong H, Blunt MJ. Pore-network extraction from micro-computerized tomography images. Physical Review E, 2009; 80: 036307.
[52] Rothman DH, Zaleski S. Lattice-Gas Cellular Automata, Cambridge University Press, 1997.
[53] Bakke S, Oren P-E. 3-D pore-scale modelling of sandstones and flow simulations in the pore networks. SPE J., 1997; 2: 136.
[54] O'Connor RM, Fredrich JT. Microscale flow modeling in geologic materials. Phys. Chem. Earth, Part A, 1999; 24: 611.
[55] Keehm Y, Mukerji T, Nur A. Permeability prediction from thin sections: 3D reconstruction and Lattice-Boltzmann flow simulation. Geophysical Research Letters, 2004; 31: L04606.
[56] Chen S, Doolen G D. Lattice Boltzmann method for fluid flows. Annual Review of Fluid Mechanics, 1998; 30: 329
[57] Succi S. The Lattice Boltzmann Equation for Fluid Dynamics and Beyond. UK Oxford University Press. 2001.
[58] Manswart C, Aaltosalmi U, Koponen A, Hilfer R, Timonen J. Lattice-Boltzmann and finite-difference simulations for the permeability for three-dimensional porous media. Physical Review E, 2002; 66: 016702.
[59] Zhang D, Zhang R, Chen S, Soll WE. Pore scale study of flow in porous media: Scale dependency, REV, and statistical REV. Geophysical Research Letters, 2000; 27: 1195.

[60] Degruyter W, Burgisser A, Bachmann O.; Malaspinas, O. Synchrotron X-ray microtomography and lattice Boltzmann simulations of gas flow through volcanic pumices. Geosphere, 2010; 6: 470.
[61] Winardhi CW, Maulana FI, Latief FDE. Permeability Estimation of Porous Rock by Means of Fluid Flow Simulation and Digital Image Analysis. International Symposium on Geophysical Issues, IOP Conf. Series: Earth and Environmental Science, 2016; 29: 012005.
[62] Qian YH, d'Humières D, Lallemand P. Lattice BGK models for Navier-Stokes equation. Europhys. Lett., 1992; 17: 479–84.
[63] Latief FDE, Fauzi U. Permeability and Tortuosity Anisotropy of a Fractured Porous Rock. 3rd International Workshop on Rock Physics, 2014; Perth, Western Australia.
[64] Xiang-Jun L, Hong-Lin Z, Li-Xi L. Digital rock physics of sandstone based on micro-CT technology. Chinese Journal Geophysics, 2014; 57, 1133.
[65] Jerauld G, Salter SJ. The effect of pore-structure on hysteresis in relative permeability and capillary pressure: Pore-level modeling. Transport in Porous Media, 1990; 5(2):103-151.
[66] Valvatne PH, Blunt MJ. Predictive pore-scale network modeling of two-phase flow in mixed wet media. Water Resources Res., 2004; 40:W07406 2004.
[67] Donaldson EC, Thomas RD, Lorenz PB. Wettability determination and its effect on recovery efficiency. SPE J., 1969; 9: 13.
[68] Anderson WG. Wettability Literature Survey - Part 2: Wettability Measurement. J. Pet. Tech., 1986; 1246.
[69] Cuiec L. Restoration of the natural state of core samples. In Paper SPE 5634 presented at the ATCE, Dallas, 1975.
[70] Cuiec L, Longeron D, Pacsirszky J. Recommendations for the determination of the wettability of a specimen of reservoir rock. Rev. Inst. Franc. Du Petrole, 1978; 33(6): 907.
[71] Donaldson EC. Oil–water–rock wettability measurement, Symposium on Chemistry of Enhanced Oil Recovery. Atlanta, 1981.
[72] Gant PL, Anderson WG. Core cleaning for restoration of native wettability. SPE Formation Evaluation Paper No. 14875 1998; 3: 131.

To whom correspondence should be addressed: Dr. Onuoha F. Wopara, Department of Petroleum Engineering, Rivers State University, Port Harcourt, Nigeria, wopara.fidelis@ust.edu.ng